Meccanica (2024) 59:1103–1119
https://doi.org/10.1007/s11012-024-01836-9

RESEARCH

Hybrid film cooling geometry analysis with OpenFOAM

Ilyes Belouddane · Mohammed Hamel · Azzeddine Khorsi

Received: 8 February 2024 / Accepted: 4 June 2024 / Published online: 3 July 2024

Abstract This paper presents a numerical investigation of the film cooling performance of a new hybrid film cooling geometry. The new hybrid concept was created to enhance the film cooling performance of gas turbine blade. The scheme consists of a converging slot hole or console with a cylindrical hole featuring a branching cylindrical hole. An analysis of the cooling performance of the advanced hybrid film cooling model was carried out across blowing ratios of (B = 0.37, 0.60, and 0.87) at a density ratio of DR=1. A numerical simulation was performed using open-source CFD software OpenFOAM. The validity of the current numerical model was evaluated for the console case, revealing excellent agreement between the numerical results and the experimental data. In this study, two distinct forms, F1 and F2, are represented with the same position variation; the SST K $-$ ω turbulence model was selected as the turbulence model for the analysis. The results show that the hybrid concepts, including auxiliary jets, enhance film cooling efficiency by effectively dispersing coolant across downstream surfaces and reducing the impact of the counter-rotating vortex pair by improving mixing with the mainstream flow. Furthermore, the supplementary jet ensures the primary coolant jet moves beside the test surface, which results in higher effectiveness, especially at high blowing ratios.

Keywords Adiabatic effectiveness · Film cooling · Gas turbine · Numerical simulation · OpenFOAM

Khorsi Azzeddine and Mohammed Hamel have contributed equally to this work.

I. Belouddane (✉) · M. Hamel · A. Khorsi
Laboratory of Applied Mechanics, Faculty of Mechanical Engineering, University of Science and Technology of Oran, Mohamed-Boudiaf (USTOMB), El Mnaouar, BP 1505, 31000 Bir El Djir, Oran, Algeria
e-mail: ilyes.belouddane@univ-usto.dz

M. Hamel
e-mail: hamel_moh78@yahoo.fr

A. Khorsi
e-mail: azzeddine_khorsi@yahoo.fr

A. Khorsi
Complex Systems Laboratory, Higher School of Electrical and Energetic Engineering, Chemin Vicinal N9, 31000 Oran, Oran, Algeria

1 Introduction

Gas turbine blades are engineered to endure high-temperature operating conditions. However, there is a limit to how high the combustion gas temperature can be raised. If the temperature exceeds the safe operating limits of the turbine blades, it can lead to material degradation, reduced blade life, and potential failure. Therefore, a balance must be struck between maximizing the gas turbine's efficiency and power output by increasing the combustion gas temperature and ensuring the long-term reliability and durability of the

turbine blades. This balance is achieved through meticulous engineering design, material selection, cooling techniques, and advanced blade coatings.

Film cooling is a critical technology widely utilized in gas turbines to protect high-temperature components from harsh operating conditions [1]. This technique involves introducing a thin layer of cool air on the turbine blade surfaces, acting as a thermal barrier to reduce heat transfer from hot gases to the blade material. Several factors must be considered to ensure the effectiveness of air film cooling performance in gas turbine applications. Bogard and Thole [2] conducted a detailed analysis of the factors influencing film cooling effectiveness, providing valuable insights into its performance. It is plausible that they classified these parameters into three distinct aspects to facilitate their analysis and discussion. These groupings might have been based on factors such as coolant injection parameters, geometric considerations, and flow conditions and the other key factors that can impact film cooling performance: turbulence levels (turbulence in the mainstream flow impacts film cooling performance). Film cooling hole shape and orientation. combust-or and aerodynamic effects. Understanding and optimizing these factors through advanced computational simulations, experimental testing, and engineering expertise are crucial for achieving efficient and effective film cooling in gas turbine applications. By meticulously considering these factors, engineers can design and implement film cooling systems that provide adequate protection and enhance high-temperature gas turbine components' overall performance and durability.

The counter-rotating vortex pair CRVP phenomenon in film cooling arises when coolant is injected through a cooling hole into the mainstream flow. As the coolant jet exits the hole, it induces a swirling motion that leads to the formation of the counter-rotating vortices. It rotates in the same direction as the mainstream flow, enhancing the mixture between the coolant and the hot gases. This mixing helps in reducing the temperature of the surface being cooled. Additionally, the vortices can cause the coolant film to separate or lift off the surface, resulting in film detachment and decreased cooling efficiency. Researchers and engineers study the characteristics and behaviour of the CRVP to optimize film cooling designs. They investigate techniques to mitigate adverse effects, such as modifying cooling hole shapes, orientations, and injection strategies. By understanding the CRVP phenomenon and its impact on film cooling, engineers can develop more efficient cooling strategies to enhance gas turbine performance and component longevity. The discussion of CRVP is pertinent in the context of JICF. Haven and Kurosaka [3] discussed the mechanisms of two vortical structures noticed in JICF, which stands for the jet in crossflow, where a fluid jet is injected perpendicular to a crossflowing stream. They were assigned titles "kidney vortices" and "anti-kidney". Another term denoting CRVP is the anti-kidney vortices, which are aimed at lessening the strength of the kidney vortices. Tyagi and Acharya [4] investigated film cooling dynamics from an inclined jet, emphasizing the importance of understanding coolant jet-crossflow interactions for gas turbine blade cooling,they highlighted the role of hairpin vortices in influencing heat transfer on the blade surface, with their results showcasing the significant impact of these vortices on mixing processes and heat transfer rates in the wake region. Jindal et al. [5] found that by optimizing the vortex generator geometries and blowing ratios, they were able to influence the formation of counter-rotating vortex pairs CRVP near the surface of the turbine blade. These CRVP played a crucial role in controlling the jet heights and promoting the lateral spreading of the cooling jets. This interaction ultimately led to a significant enhancement in film cooling effectiveness, showcasing the importance of these variables in the cooling process. Jiang et al. [6] demonstrated that the effectiveness of film cooling on turbine blades is critically affected by the configuration of cooling holes, with different shapes yielding varied thermal protection. Specifically, they found that the hole's geometry has a significant impact, with expanded holes providing enhanced cooling compared to cylindrical ones, especially at elevated blowing ratios. Furthermore, they observed that at a higher blowing ratio, the vortex pairs—kidney-shaped vortices inherent to jet-in-crossflow scenarios—increase strength, leading to more extensive lateral spreading of cooling effectiveness. Their study also indicated that the interaction of flows between adjacent rows of cooling holes plays a vital role in the overall film cooling effectiveness, where closely spaced double rows can greatly improve surface cooling by ensuring a more cohesive coolant film, even under complex blade rotation and curvature conditions. Jindal et al.

[7] explores the effects of different hole shapes, orientations, and arrangements on film cooling effectiveness. Through computational analysis, this study compares five distinct hole shapes cylindrical, elliptic, triangular, semi cylindrical, and semi elliptic over a range of blowing ratios from 0.67 to 1.67. While the triangular geometry showed superior cooling effectiveness, the semi-elliptic shape achieved the best balance between cooling effectiveness and coolant mass consumption. This detailed analysis of film cooling extends to variations in hole orientation and the number of rows, offering new insights into optimising thermal management strategies for combustion chamber walls and turbine blades, potentially influencing future designs in aeronautical and space science applications. Runzhou Liu et al. [8] explored the impact of blowing ratio and film hole placement on turbine blade cooling effectiveness. They highlighted the significant role of bore cooling in specific regions and observed a shift in cooling dynamics with varying blowing ratios. At lower blowing ratio, film cooling dominated, but bore cooling became more influential as the ratio increased, eventually surpassing film cooling at the highest ratio tested. These findings provide crucial insights for optimizing turbine blade cooling systems. Jindal et al. [9] investigated enhancing film-cooling effectiveness using mixed hole arrangements on a 3D flat plate. Their study focused on staggered rows with triangular and semi-elliptic-shaped holes. Results showed improved cooling efficiency due to significant merging of coolant jets, weakening of vortex pairs, and the identification of an optimal hole arrangement (M.R. VI) for maximizing cooling effectiveness. Abdala et al. [10] investigated the impact of blowing ratio on film cooling effectiveness in narrow trench configurations. They observed that varying the blowing ratio (ranging from 0.5 to 1.4) significantly affected the predicted film cooling performance within the trench. Additionally, the researchers compared the performance of different turbulence models ($k-\epsilon$, $k-\omega$, SST Gamma Theta) in predicting film cooling effectiveness. The $k-\omega$ SST turbulence model yielded superior results in predicting film cooling effectiveness in narrow trench configurations. This turbulence model demonstrated enhanced accuracy and reliability compared to other models, especially in capturing the complex flow dynamics within the trench. By utilizing the $k-\omega$ SST model, the researchers achieved more precise predictions of film cooling performance, highlighting the model's effectiveness in simulating the intricate interactions between the coolant flow and the surface. These results underscore the importance of selecting the appropriate turbulence model, such as the $k-\omega$ SST model, to improve the predictive capabilities of computational simulations in optimizing film cooling strategies for gas turbine components. Acosta et al. [11] conducted a study comparing the $k-\omega$ SST model, $k-\varepsilon$ model, and experimental data for film cooling on a flat plate with a multi-exit hole configuration, the $k-\omega$ SST model was identified as providing the most accurate predictions for the temperature distribution along the external surface. This finding underscores the effectiveness of the $k-\omega$ SST model in capturing the complex flow behaviour and heat transfer characteristics associated with film cooling applications on flat plates with multi-exit hole configurations. Sargison et al. [12] first conducted experimental research on a novel style of film cooling hole known as a console (CONverging Slot-hOLE). This finding indicates that the converging slot-hole design effectively enhances the distribution of the coolant film, resulting in improved cooling performance. The study demonstrated that the console hole exhibited a significantly higher coolant film coverage rate than the cylindrical and fan-shaped holes.

The present study introduces an innovative hybrid film cooling design based on the "console (CONverging Slot-hOLE)", which has been conceived and developed in previous studies [12]. This advanced cooling system enhances the primary configuration by incorporating a cylindrical jet hole, representing a state-of-the-art hybrid cooling approach. The investigation delves into how the positioning of the supplementary branch jet injection and blowing ratio influence film cooling performance and flow structure. Five different configurations are studied under three blowing ratios (B = 0.37, 0.60, 0.87). The results of these cases are compared with the reference "console", a proposed open-source CFD model based on OpenFOAM used for discussion. Additionally, the study highlights that OpenFOAM has significantly produced reliable simulation outcomes that demonstrate strong validation against experimental data.

2 Methods

In the present study, the computational domain for numerical simulations is referred to the experimental of Sargison et al. [12].

Figure 1a displays schematic illustrations of the three-dimensional computer system used in this research. The flow channel has a length of 32.5 d and a height of 8 d. The plenum has dimensions 6 d, 2.5 d, and 3 d, respectively. The distance from the leading edge of the hole outlet to the mainstream inlet is 7.5 d, and the spanwise distance (p/d) is 3 d. The console inlet and is taken as 25 mm. Figure 1b shows the basic console configuration. The compound concept was chosen as the newly shaped hole, named CCH, presented in Fig. 1c and the geometry details are in Table 1. The distance along the x-direction between the primary film cooling hole and an additional hole is represented by the parameter λ. In the presentation of data, the equivalent cylindrical hole diameter of d = 20 mm was utilized, as Sargison et al. [12].recommended. Five different geometries were studied with different positions, and they are represented in Table 2:

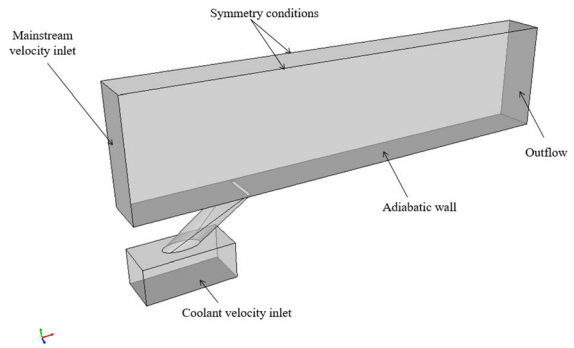

(a) Three-dimensional view and boundary conditions

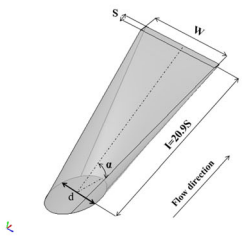

(b) Basic console.

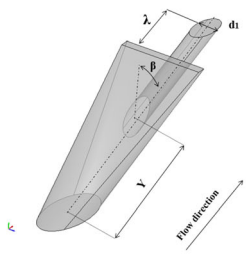

(c) Hybrid film cooling geometry.

Fig. 1 Description of studied

2.1 Boundary conditions

The details of boundary conditions in the OpenFOAM (open-source field operation and manipulation) environment are shown in Fig 1a; the inlet of the mainstream was specified as a velocity-inlet with a velocity of U = 26 m/s with a 1% inlet turbulence intensity, according to the experience of Sargison et al. [12]. The pressure equality at the outflow of both the mainstream and secondary flows is zero bar; the boundary conditions applied to the wall surface of the flat plate included the no-slip condition for velocity, meaning that the velocity of the fluid at the wall is zero. The adiabatic state for temperature implies no heat transfer between the wall and the fluid. Similar conditions were applied to the inside wall of the CCH and the plenum. The density ratios DR = 1 and T_c/T_∞ = 1.06 are the ratio of coolant temperature to free-

Table 1 Test plate details (depending on Fig. 1b, and c)

Configuration	$d1/d$	λ (d)	β (°)	α(°)	W (d)	S (d)
Baseline console	–	–	–	35	2.5	0.25
F1-CCH	0.75	2	62	35	2.5	0.25
F1-CCH	0.75	3	73	35	2.5	0.25
F2-CCH	0.5	2	62	35	2.5	0.25
F2-CCH	0.5	3	73	35	2.5	0.25

Table 2 Different computational models

Cases	Description
Case 1	Geometric parameters from Sargison et al. [12]
Case 2	Forme 1 (F1-CCH) with λ=2 d
Case 3	Forme 1 (F1-CCH) with λ=3 d
Case 4	Forme 2 (F2-CCH) with λ=2 d
Case 5	Forme 2 (F2-CCH) with λ=3 d

stream, and three blowing ratios are considered in this study: B = 0.37, 0.60, and 0.87. for each geometry blowing ratio (B) is defined as:

$$B = \frac{\rho_c \cdot u_c}{\rho_\infty \cdot u_\infty} \quad (1)$$

where ρ_∞ and u_∞ are the density and velocity of the mainstream, respectively, and u_c is the average velocity of the outlet of the film cooling hole, the inlet coolant velocity can be simply calculated using continuity equation.

2.2 Turbulence modelling

The simulations were performed using the OpenFOAM software. In the solver package, the solution of the Reynolds-averaged Navier–Stokes equations is obtained by using the finite volume method to discretize the continuity, momentum, and energy equations; the second-order upwind solution scheme is used to solve the momentum, energy, and turbulence model equations; the pressure–velocity coupling is achieved using the SIMPLEC algorithm of Van Doormal and Raithby [13], and the calculation is continued until the convergence criterion 10^{-6} is met. In this study, the turbulence is modelled by a shear stress transport model (SST) of Menter [14], and the OpenFOAM variant is based on the 2003 model. the SST k-omega turbulence model is a two-equation eddy-viscosity model that is used for many turbomachines applications, model which has become very popular, formulation blends the best of both worlds, it is a hybrid model combining the Wilcox [15]. k $-$ ω and the k-ϵ models, this model is known to provide a good compromise by combining the k $-$ ω model of Wilcox [15] in the near the wall region, and the high Reynolds k- ϵ model in the outer region, Alternatively, the k $-$ ω- SST is a hybrid model that combines the advantages of the k $-$ ω and k-ϵ models by switching between them, the initial grid elements are situated at y^+ less than 2, and in the fully turbulent region is the k $-$ ϵ model, this model depicts flow separation more efficiently than other eddy viscosity models under unfavourable pressure gradients, and thus the more accurate prediction of near-wall turbulence, an essential factor in turbulent heat transfer predictions, and has been confirmed by many investigations [16]. The $k - \omega$ SST model excels in predicting boundary layer characteristics, which is crucial for capturing the flow dynamics near the surface in film cooling applications. This capability helps accurately simulate the interaction between the coolant jet and the mainstream flow [10]. the $k - \omega$ SST model is designed to accurately predict the behaviour of fluid flow and heat transfer in complex geometries, making it well-suited for film cooling simulations [17]. It can accurately predict the laterally averaged and centerline film cooling effectiveness, as demonstrated in [17], which compares the performance of the $k - \omega$ SST model with experimental measurements for a flat plate film cooling system.

2.3 Mesh generation and validation analysis

The calculation grid was created using Salome, an open-source library for volume mesh generation. Overall, unstructured tetrahedral grids were generated for the entire computational domain, as shown in Fig. 2. The mainstream zone is partitioned into a near-wall region and a far-away-wall region. Specifically, a layer of locally structured grids is produced near the wall surface, employing a hexahedral mesh. Grid density near the console exit and the plaque was refined to accurately resolve unsteady flow features and the interaction between the coolant and free stream, enhancing the precision of the simulation.

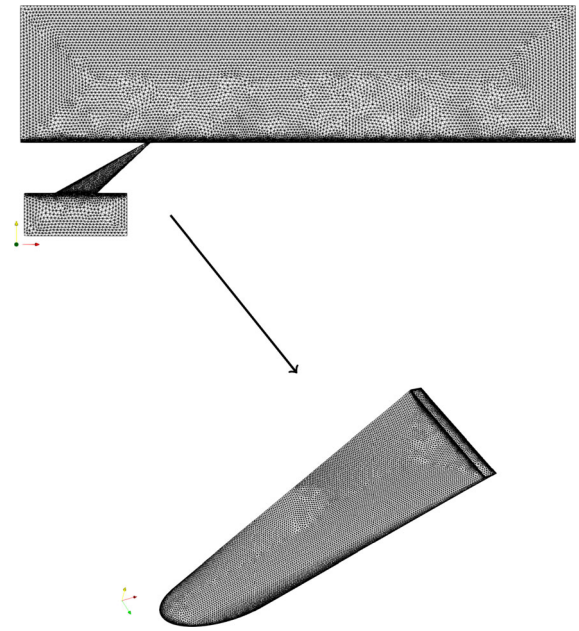

Fig. 2 Computational grid

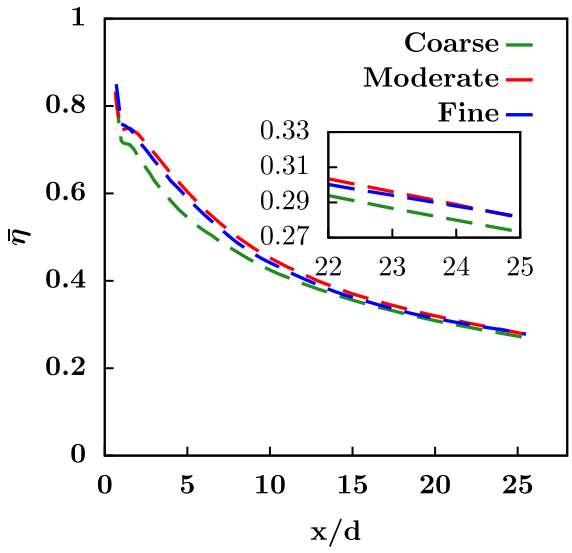

Fig. 3 Sensitivity analysis—laterally averaged film cooling effectiveness for three different meshing

Three types of unstructured tetrahedral meshes are coarse, medium, and fine. To determine the optimal grid number, the laterally averaged adiabatic film effectiveness at B = 0.60 is employed to verify the independency of grid numbers. As shown in Fig. 3, the cooling effectiveness curves for grid sizes of 1.0 million and 1.5 million cells overlap significantly, with an average error of only 6.94%. In contrast, the average error between the results for 0.5 million and 1.0 million meshes is higher at 11.08%, as illustrated Fig. 4. Therefore, a grid size of 1.0 million cells was chosen for this study. The assessment of mesh quality

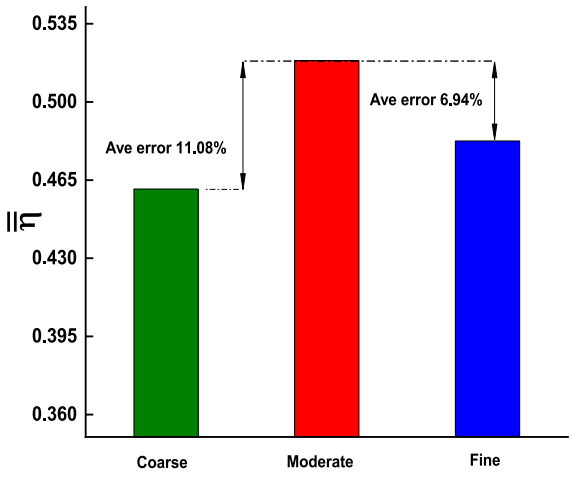

Fig. 4 Analysis of grid independence

parameters was conducted using the checkMesh tool in OpenFOAM. This confirmed a well-defined mesh boundary and volume. The aspect ratio indicated acceptable element shape variations, while non-orthogonality and skewness metrics were within acceptable limits. Moreover, the implementation of 18 inflation layers, along with adjusting the initial layer thickness, helped improve mesh quality near the wall.

3 Result

3.1 Laterally averaged adiabatic film cooling effectiveness

To enable comparisons, Eq. (2) a non-dimensional temperature called adiabatic film cooling effectiveness, which ranges from one to zero. Equation (3) defines a laterally averaged adiabatic film cooling effectiveness, presenting a comprehensive perspective on the cooling mechanism in the spanwise direction for subsequent discussions.

$$\eta = \frac{T_{aw} - T_{\infty}}{T_c - T_{\infty}} \tag{2}$$

$$\bar{\eta} = \frac{1}{L}\int_0^L \eta(z)\,\mathrm{d}z \tag{3}$$

L is the span-wise dimension of the plate, T_{aw} is the temperature on the test plate, where T_{∞} and T_c are the mainstream and the coolant temperatures, respectively.

3.2 Experimental validation comparison with previous results

The cooling effectiveness results obtained from the current study were compared with the experimental data of Sargison et al. [12]. To confirm the accuracy and validity of the computational approach used in this research, as presented in Fig. 5. The computational and experimental data were generated using identical geometry, and the boundary conditions applied in the simulations were similar to those used in the experiments conducted by Sargison et al. [12]. According to Fig. 5, These findings exhibit an excellent agreement with experimental data, especially considering the results obtained using OpenFOAM. Showcasing the

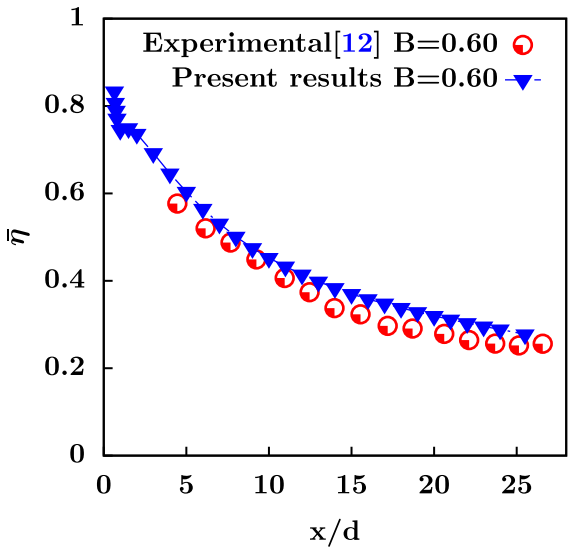

Fig. 5 A comparison between the current numerical results and the experimental data of Sargison et al. [12]

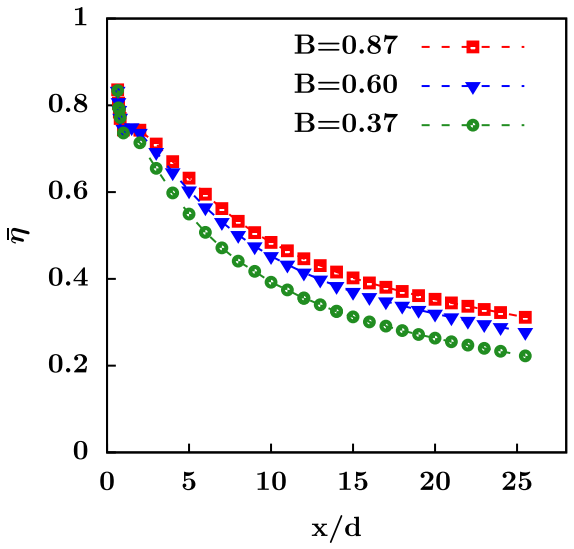

Fig. 6 Laterally averaged effectiveness results: case (1) at B = 0.37, B = 0.60, B = 0.87

high accuracy of film cooling numerical prediction using the OpenFOAM Code that provides trustworthy and realistic results. In summary, the statement highlights the success and effectiveness of OpenFOAM in generating simulation results that closely match experimental observations. It underscores the software's capability to provide reliable and accurate simulations in this study.

3.3 Effect of blowing ratio

Figures 6, 7, and 8 illustrate the effect of the blowing ratio on the lateral-averaged cooling effectiveness for different blowing ratios (B = 0.37, 0.60, and 0.87). The data analysis reveals a consistent trend across all configurations studied, indicating that the lateral-averaged film cooling efficiency initially increases near the jet outlet and subsequently decreases along the x/d direction. A notable enhancement in cooling effectiveness is observed near the jet outlet, where the coolant flow is concentrated with higher momentum. However, as the coolant progresses downstream, it disperses and interacts with the mainstream flow, resulting in a gradual decline in effectiveness. The evolution of the boundary layer and the thermal mixing between the coolant and mainstream flow are key factors contributing to the reduction in cooling efficiency along the (x/d > 0) direction.

Figure 6 illustrates significant variations in average span-wise film cooling effectiveness at specific locations (x/d = 5, x/d = 15, and x/d = 24) across different blowing ratios. Particularly, blowing ratios of 0.87 and 0.60 exhibit notable differences in film cooling effectiveness compared to the case with a blowing ratio of 0.37. Initially, at x/d = 5, B = 0.60 is 9.91% higher, and B = 0.87 is 15.06% higher than B = 0.37. Moving to x/d = 15, the lead for B = 0.60 increases to 18.49%, and for B = 0.87, it rises to 28.86%. Finally, at x/d = 24, the differences peak with B = 0.60 at 23.78% and B = 0.87 at 38.26% above B = 0.37. This trend indicates that as the blowing ratio increases, the lateral-averaged adiabatic film cooling effectiveness $\bar{\eta}$ of the console initially rises and then decreases, with the optimum blowing ratio around 0.60 and 0.37, respectively. The increased blowing ratio enhances the coolant's momentum, allowing for deeper penetration into the hot gas stream and significantly improving heat transfer.

In Fig. 7a,film cooling effectiveness increases noticeably for blowing ratios of 0.60 and 0.87, starting at 10.56% and 16.66% higher than B = 0.37, respectively. At x/d = 15, these differences amplify, with B = 0.60 showing a 21.32% improvement and B = 0.87 demonstrating a significant 35.28% enhancement over B = 0.37. This trend continues at x/d = 24, where the disparities widen further, with B = 0.60 at 28.70% and B = 0.87 at an impressive 49.64% above B = 0.37.

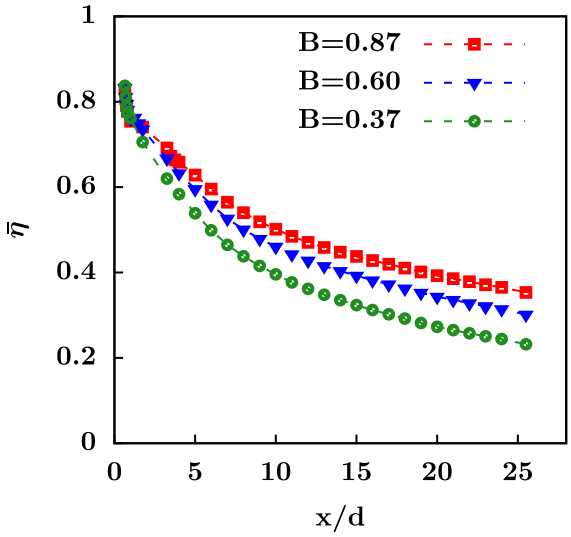

(a) Case 2

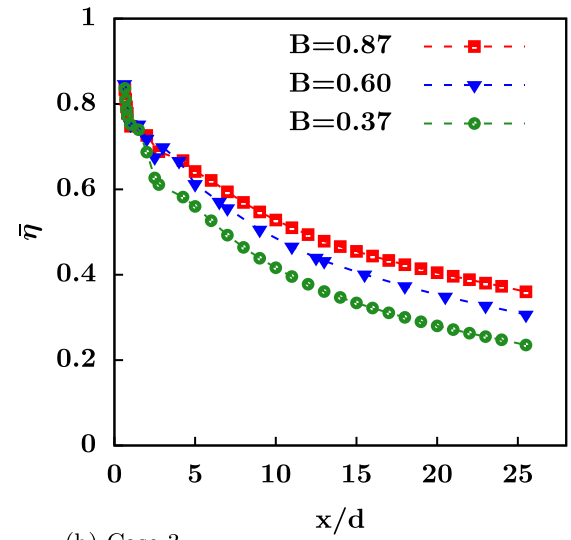

(b) Case 3

Fig. 7 Laterally averaged effectiveness results: case (2–3) at B = 0.37, B = 0.60, B = 0.87

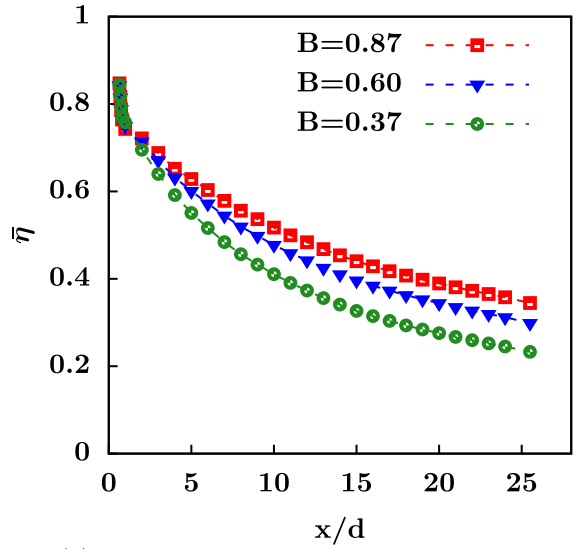

(a) Case 4

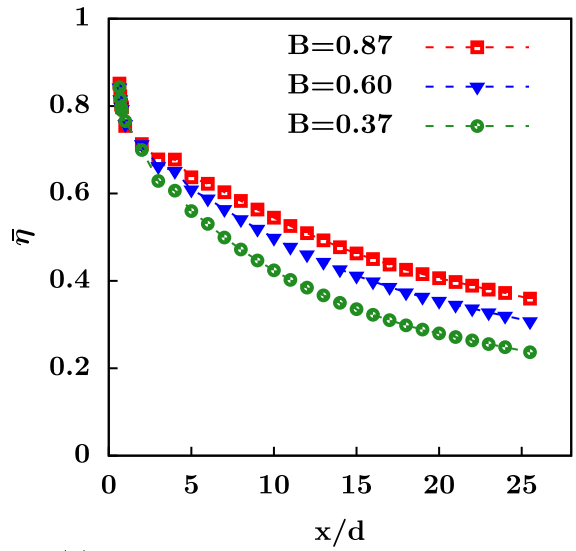

(b) Case 5

Fig. 8 Laterally averaged effectiveness results: case (4–5) at B = 0.37, B = 0.60, B = 0.87

These findings underscore a strengthening effect of the blowing ratio along the test surface, particularly pronounced at B = 0.60 and B = 0.87, showcasing the impact of momentum flux ratio variations. Despite the inherent challenges related to jet heights and lateral spreading, it is evident that higher blowing ratios result in a more extensive spread of the secondary flow over downstream surfaces in the hybrid scheme, leading to a notable enhancement in film cooling performance. Furthermore, using an auxiliary jet to guide the main jet along the test surface proves particularly effective, especially at elevated blowing ratios.

The results depicted in Fig. 7b consistently show that blowing ratios of 0.60 and 0.87 outperform a blowing ratio of 0.37 along the test surface, indicating a growing impact of high blowing ratios that disproportionately affect these specific points of analysis. While the differences are initially subtle at x/d = 5,

they progressively widen, particularly pronounced at x/d = 24, with B = 0.87 showcasing a significantly more robust response than B = 0.60. The F1 configuration of the film cooling holes plays a pivotal role in directing the coolant jets at precise angles towards the surface. This optimized orientation effectively minimizes jet lift-off by ensuring closer proximity of the coolant flow to the surface, thereby reducing the risk of inadequate cooling coverage associated with elevated blowing ratios.

In Fig. 8a, the comparison of blowing ratios B = 0.37, B = 0.60, and B = 0.87 reveals a substantial increase in differences as x/d> 0,indicating that higher blowing ratios, particularly B = 0.60 and B = 0.87, exert a more significant influence on cooling performance by affecting the momentum and penetration of the coolant jets into the mainstream flow compared to B = 0.37. This trend is further supported by the analysis in Fig. 8b at λ = 3d, where the divergence in growth rates across the test surface consistently intensifies for datasets B = 0.37, B = 0.60, and B = 0.87. Notably, at x/d = 5, 15, and 24, the disparities between B = 0.60 and B = 0.37, and B = 0.87 and B = 0.37 exhibit a notable widening trend, indicating a progressive strengthening of the influence of higher blowing ratios (B = 0.60 and B = 0.87) compared to B = 0.37. In summary, the blowing ratio plays a crucial role in shaping film cooling performance, with high blowing ratios significantly impacting coolant coverage, penetration, adhesion, momentum, and heat transfer, enhancing cooling efficiency across the test surface.

3.4 A comparative analysis of various cases

Figure 9 compares the centre-line film cooling effectiveness for different configurations at the same blowing ratio. Across all blowing ratios (B = 0.37, B = 0.60, and B = 0.87), the trend indicates an increase in film cooling effectiveness near the jet outlet, followed by a decrease along the axial distance (x/d).

At a low blowing ratio of B = 0.37, as depicted in Fig. 9a, the converging round-to-slot hole exhibits the lowest performance relative to the other configurations. The observation suggests that the quantity of coolant injected into the mainstream flow is insufficient to ensure effective cooling coverage across the surface. Consequently, this deficiency in coolant supply can lead to reduced cooling effectiveness and potentially result in insufficient heat transfer protection.

When examining the F1 configuration at $\lambda = 2$ and λ = 3, a notable enhancement in the film cooling effectiveness is observed, with increases of approximately 40.94% and 40.91% above the baseline, respectively, this significant deviation from the baseline indicates a substantial modification that increases η by almost half of the baseline value. Introducing a secondary flow plays a crucial role in stabilizing the coolant layer near the surface, mitigating the risk of jet lift-off, and ensuring efficient cooling across the film-cooled surface, enhancing heat transfer efficiency. In contrast, systems lacking a secondary flow may exhibit less uniform coolant distribution along the surface, potentially leading to uneven cooling and hot spots.

Moreover, the F2 model demonstrate a different trend in film cooling effectiveness. While still outperforming the baseline, shows a slightly less pronounced increase in film cooling effectiveness compared to the F1 configuration, with F2 $\lambda = 2$ and F2 $\lambda = 3$ exhibiting increases of approximately 24.98% and 23.62%, respectively the reduced-diameter secondary holes in the F2 configuration limit cooling coverage due to their reduced surface area and lower coolant flow rates compared to the larger diameter of the secondary flow in F1, results in a more significant impact on coolant jet behaviour and distribution in F1. Both F1 $\lambda = 2$ and F1 $\lambda = 3$ yield very similar average results 59.45% and 59.54%, respectively, while F2 λ = 2 and F2 λ = 3 average at 54.16% and 52.86%, indicating that the placement of auxiliary holes in F1 and F2 contributes to a uniform coolant distribution and consistent cooling effects along the centerline. Additionally, variations in hole orientation (λ = 2 and λ = 3) were found not to significantly affect centerline cooling effectiveness.

As shown in Fig. 9b for B = 0.60, the advantages of integrating larger auxiliary film cooling holes (F1) and smaller auxiliary holes (F2) over the basic design are evident in their enhanced effectiveness, suggesting that the modifications introduced in F1 and F2 were successful in improving outcomes. The notable differences observed between the console and F1 and F2 datasets (ranging from 25% to 44%) indicate distinct configuration variations. Consoles displaying significantly lower normalized results than other datasets suggest potentially lower efficacy. The minimal

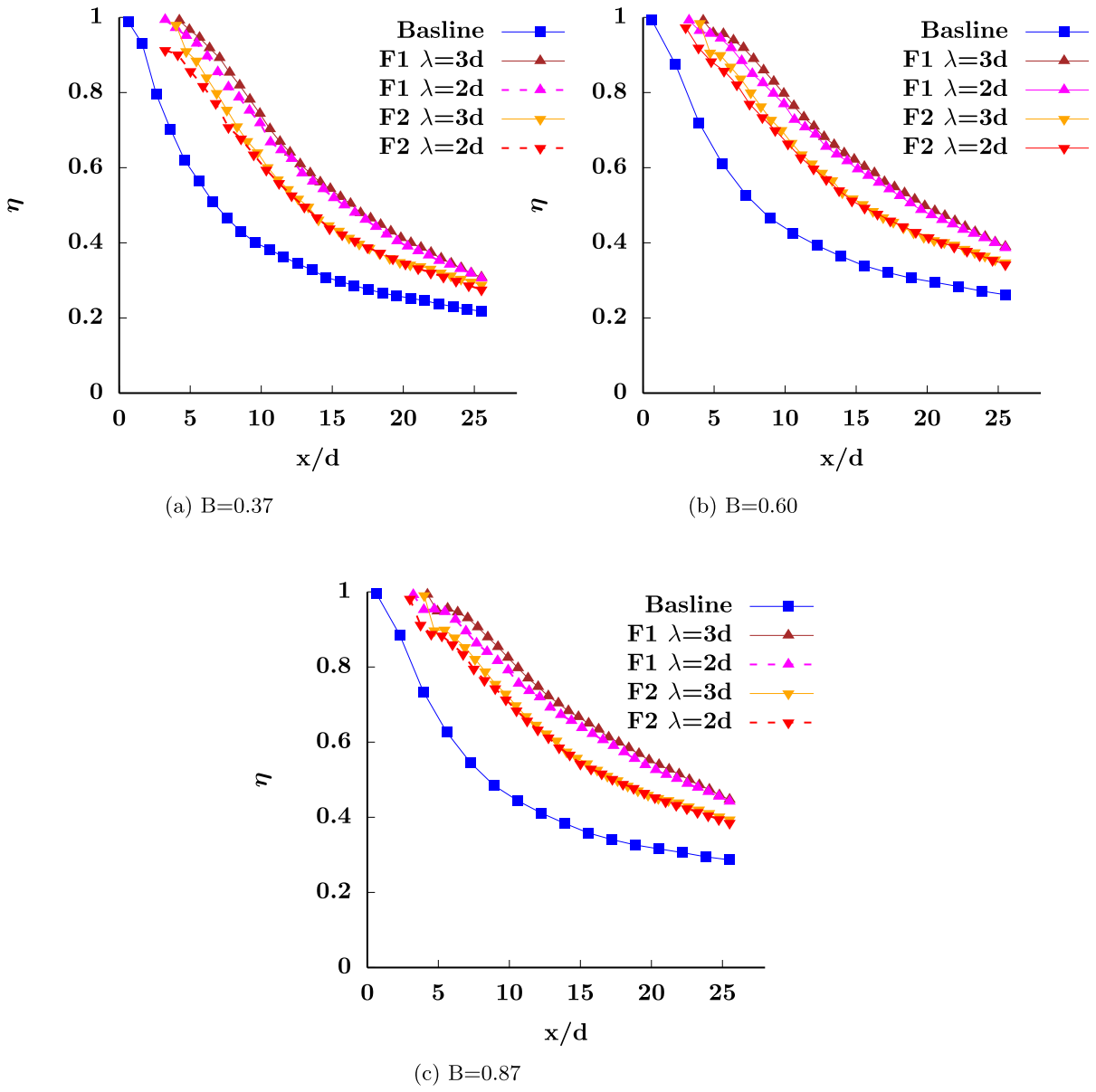

(a) B=0.37 (b) B=0.60

(c) B=0.87

Fig. 9 Centerline film cooling effectiveness for different cases with various blowing ratios

percentage variances between F1 $\lambda = 2$ and F1 $\lambda = 3$ (0.16%), and the relatively slight difference between F2 $\lambda = 2$ and F2 $\lambda = 3$ (2.43%) suggest similar cooling characteristics in terms of jet penetration depth, spreading angle, and coverage area. The film-covered area of F1 exceeds that of F2 and the baseline. The larger holes in F1 exhibit a more uniform and consistent flow distribution at their exit, fostering a stable and even cooling effect. Their enhanced ability to penetrate the boundary layer facilitates more efficient mixing with hot gases.

At B = 0.87, Fig. 9c reveals significant variations in efficacy between the baseline and the subsequent F1 and F2 configurations, with F1 showing improvements of approximately 43% to 45%, and F2 exhibiting a 27% to 28% increase in mean results. The slight changes in cooling effectiveness seen when modifying the arrangement of film cooling holes in case 3 and

case 4, with a slight 1.25% increase for case 1 and a 0.60% decrease for case 2. Implementing dual jets not only expands cooling coverage by dispersing coolant across a wider surface area but also promotes more uniform cooling and diminishes hot spots. Moreover, the dual jets boost heat transfer capabilities by elevating the coolant mass flow rate, facilitating enhanced surface heat extraction. This process leads to lower surface temperatures, improved component durability, and overall efficiency in the cooling mechanism.

3.4.1 Lateral adiabatic film cooling effectiveness

Figure 10 presents the lateral film cooling effectiveness for five configurations with different blowing ratios at the x/d = 6 plane.

At a low blowing ratio of B = 0.37, as depicted in Fig. 10a, the F1 model, specifically with λ=2 and 3, exhibits the most significant enhancements in peak η values compared to the baseline. Among these, the F1 configuration with λ = 3 shows the most substantial improvement, with a peak η approximately 3.02% higher. While the F2 configurations also show improvements over the baseline, the enhancements are more modest than the F1 model. This underscores the pivotal role of the secondary hole in augmenting film cooling effectiveness by influencing flow dynamics and optimizing cooling jet coverage. Analyzing the results at z/d = 0 and within the range of $z/d \leq -0.5$ to $z/d \geq 0.5$, the console configuration demonstrates a positive change with a +2.24% increase, indicating a more effective spread of coolant flow from the centreline, leading to enhanced coverage at the surface edges. In contrast, the other models, including F1 $\lambda = 2$ (−20.83%), F1 $\lambda = 3$ (−19.58%), F2 $\lambda = 2$ (−18.47%), and F2 $\lambda = 3$ (−17.52%), exhibit significant reductions in effectiveness. These reductions, particularly at the lateral of the cylindrical hole (z/d = 0), can be attributed to the concentration of coolant in the secondary hole, which enhances localized cooling. When insufficient coolant is present in the lateral direction, as the coolant disperses towards z/d = ± 0.5, the coverage and effectiveness of the cooling jet may decrease. This inadequate coolant distribution can result in regions of the surface receiving less cooling than desired, leading to decreased overall effectiveness of the film cooling system.

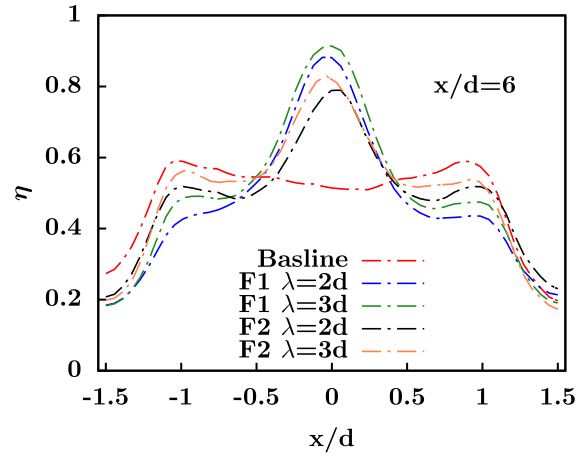

(a) B=0.37

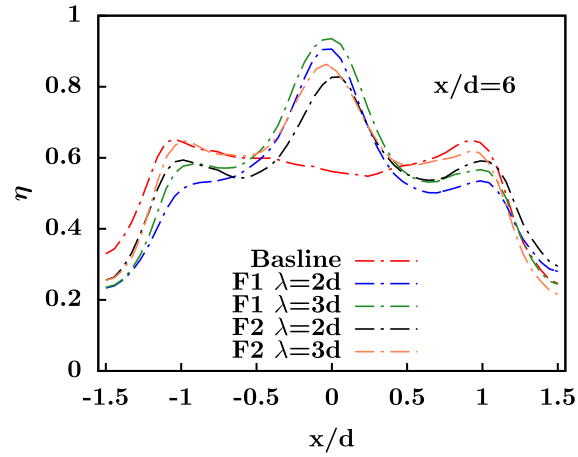

(b) B=0.60

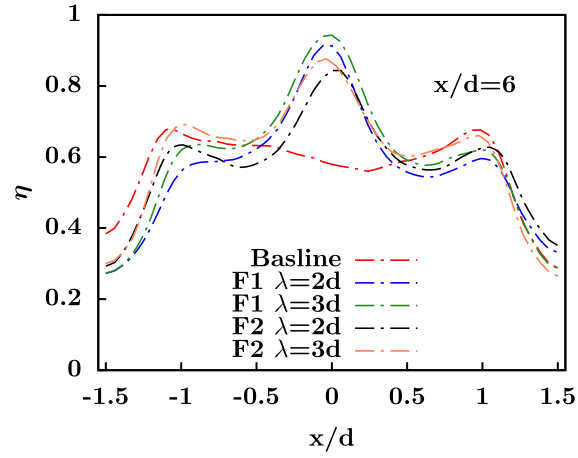

(c) B=0.87

Fig. 10 Lateral film cooling effectiveness at plane x/d = 6 with various blowing ratios

Moving to the blowing ratio B = 0.60, a similar trend is observed, as depicted in Fig. 10b. The baseline shows a slight increase of approximately +1.82% within this interval, indicating that the lateral movement of the coolant jet away from the injection point facilitates better mixing with the mainstream flow, thereby improving cooling coverage and effectiveness towards $z/d \leq -0.5$ and $z/d \geq 0.5$. Conversely, the other configurations, including F1 λ = 2 (−19.80%), F1 $\lambda = 3$ (−18.14%), F2 $\lambda = 2$ (−17.11%), and F2 $\lambda = 3$ (−15.57%) demonstrate significant reductions due to jet spreads along the center-line.

At a blowing ratio B = 0.87, as illustrated in Fig. 10c, the console configuration exhibits a moderate rise of around +2.08% within this range, indicating a consistent or gradually rising pattern at z/d = 0. In contrast, the other datasets, including F1 λ = 2 (−18.83%), F1 λ = 3 (−16.98%), F2 λ = 2 (−16.39%), and F2 $\lambda = 3$ (−14.54%).

Increasing the blowing ratio has a notable impact on lateral film cooling effectiveness, which is consistent with the previously discussed trend. Figure 10. As the blowing ratio rises, more coolant is introduced through the cooling holes, forming a more extensive and efficient coolant film along the surface. In the console configuration, the response to escalating blowing ratios at $z/d = 0$ demonstrates a progression from 0.514 at $B = 0.37$ to 0.561 at $B = 0.60$, indicating a percentage increase of approximately 9.15%. This trend persists up to $B = 0.87$, reaching a value of 0.580, reflecting a further increase of around 3.22%. At $z/d \geq 0.5$, the percentage increase from $B = 0.60$ to $B = 0.87$ is approximately 6.39%.

In the analysis of F1 with $\lambda = 2$ and 3, marginal values increase at $z/d = 0$ with varying blowing ratios (B). Specifically, for $\lambda = 2$, the value ascends from 0.880 at $B = 0.37$ to 0.913 at $B = 0.87$. A more substantial increase is noted for broader intervals ($z/d \geq 0.5$). Similarly, in the F2 configuration, significant enhancements are evident in wider intervals ($z/d \geq 0.5$) for both cases 4–5.

Figure 11 illustrates the variation in lateral cooling effectiveness at x/d = 20. The trend depicted shows a gradual decline in effectiveness with increasing distance from the cooling hole. This reduction can be attributed to a complex interplay of factors, including jet mixing with the mainstream flow, boundary layer growth, flow reattachment and separation, jet decay, and alterations in heat transfer dynamics. The

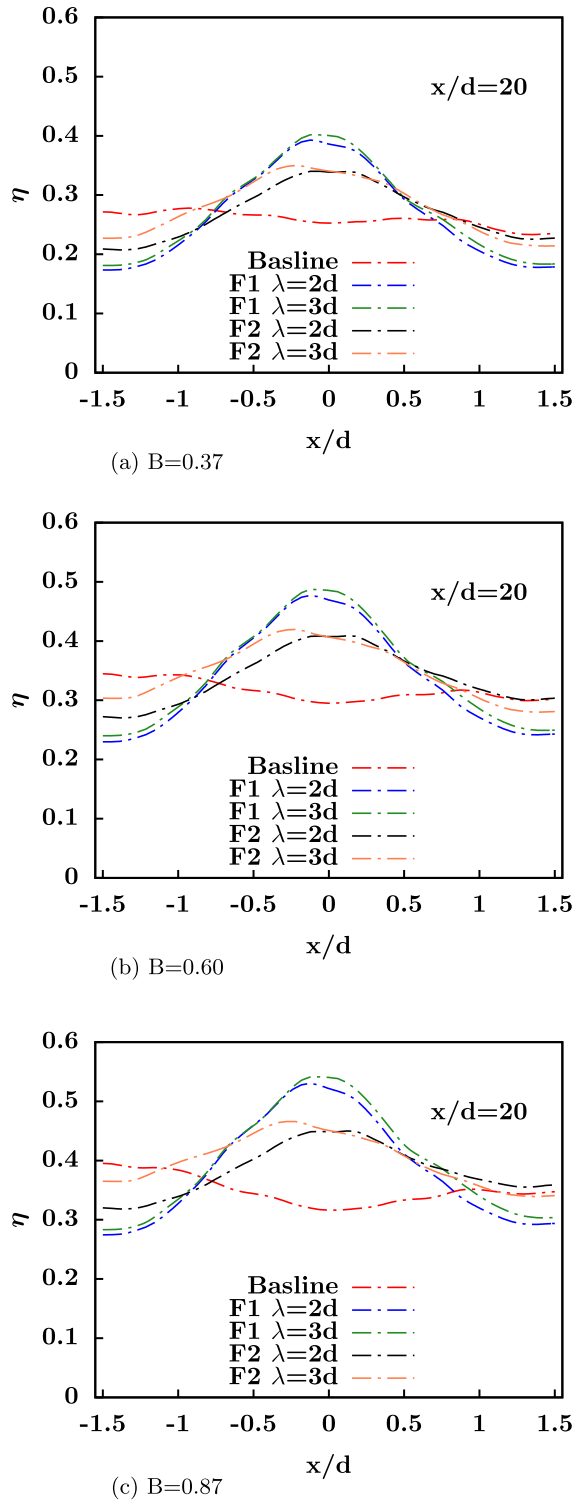

Fig. 11 Lateral film cooling effectiveness at plane x/d = 20 with various blowing ratios

diminishing effectiveness underscores the challenges of maintaining efficient heat extraction and surface cooling over extended downstream distances. As the cooling jets travel downstream, they undergo mixing and dilution with the mainstream flow, leading to a decrease in coolant concentration near the surface and a subsequent decline in heat extraction capability. Moreover, developing the boundary layer along the surface is a thermal barrier, hindering heat transfer efficiency. Changes in flow patterns, such as reattachment and separation, disrupt the smooth flow of coolant, influencing heat transfer dynamics and impacting cooling effectiveness. Additionally, jet decay and dispersion reduce momentum and cooling capacity as the jets move away from the injection point. The evolving interactions among the cooling jets, mainstream flow, boundary layer development, and heat transfer mechanisms collectively contribute to the observed decrease in cooling effectiveness over increasing axial distances in the cooling system. Figure 11 corroborates the previous findings regarding the coolant distribution along the test surface.

3.5 Wall cooling efficiency

The analysis of wall cooling effectiveness, focusing on $\eta > 0.5$, as shown in Fig. 12 for all configurations at B = 0.87, provides valuable insights into flat plate film cooling. The results in Fig. 12 highlight the effectiveness of the hybrid model; this configuration demonstrates a significantly higher proportion of high-efficiency cooling surface, particularly where the film cooling effectiveness (η) exceeds 0.5 across the total surface area. The increased value emphasizes the success of localized cooling in critical regions, as the novel design effectively reduces jet lift-off, ensuring prolonged contact time of the jet with the surface. Notably, Cases 3 and 5 exhibit substantially higher values than Cases 1, 2, and 4. The console configuration yields the lowest cooled area effectiveness, attributed to a limited coverage expansion of the cooling film along the centre-line direction. However, the specialized cooling surface ratio for cases 3 and 5 remains relatively consistent.

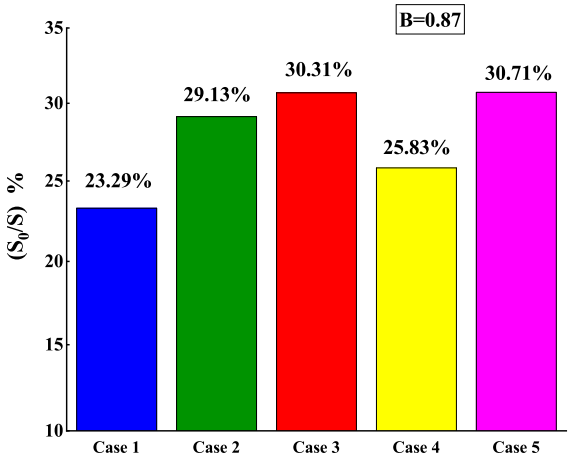

Fig. 12 Analyzing the specialized cooling surface ratio at a blowing ratio of 0.87 for different configurations and orientations

3.6 Contours of flow characteristics

Figure 13 illustrates the film cooling effectiveness distribution for the novel hybrid scheme and the conventional converging slot hole configurations at high and low blowing ratios in linear trajectory scenarios (Baseline, F1, F2), showcasing various

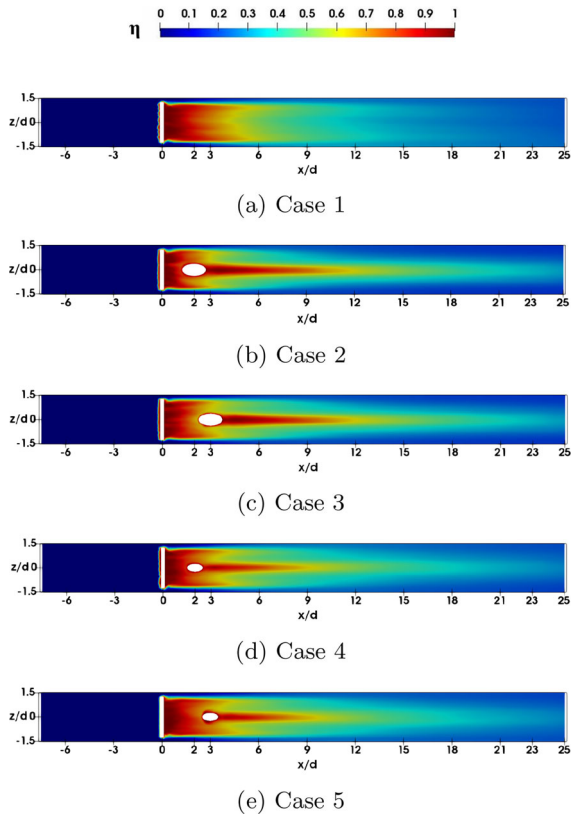

Fig. 13 Film cooling effectiveness contours downstream the wall under blowing ratios B = 0.37

locations for the innovative design. Notably, the film cooling effectiveness near the outlet jet consistently exhibits high values but lacks uniform distribution across the plate, gradually decreasing as the distance from the hole outlet (x/d) increases. Figure 13 at low blowing ratios (B=0.37), the branch jet design shows superior cooling along the streamwise direction, highlighting the benefits of supplementary holes for precise coolant flow control. In contrast, traditional configurations Fig. 13a show reduced effectiveness in this direction. Supplementary holes in a branch jet design enhance cooling efficiency by directing coolant to specific areas, improving heat transfer, lowering surface temperatures, and preventing thermal damage. Figure 14 with a high blowing ratio of 0.87, a pronounced interaction between the coolant and mainstream flow within the console configuration results in non-uniform cooling and insufficient coverage downstream, potentially leading to localized hot spots on the surface. In contrast, the hybrid design offers a more uniform cooling effectiveness distribution, ensuring enhanced surface protection and overall cooling system efficiency. The F1 model demonstrates

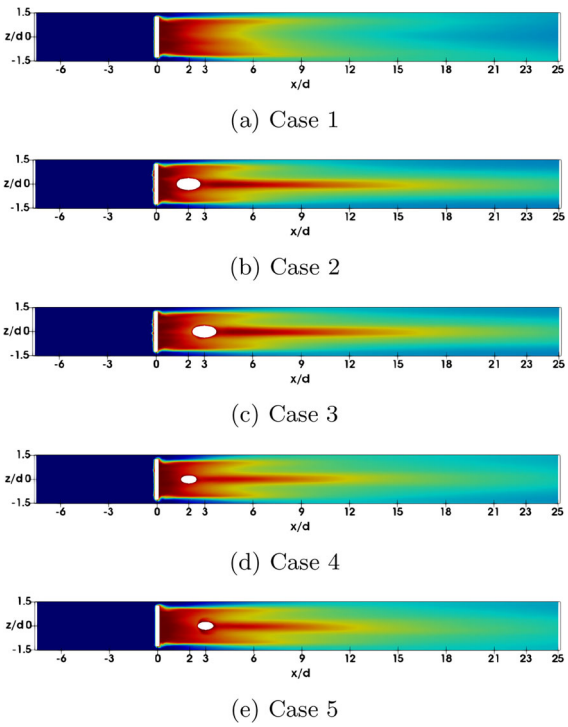

Fig. 14 Film cooling effectiveness contours downstream the wall under blowing ratios B = 0.87

heightened cooling performance along the centre-line, while the F2 variant excels in the lateral spreading of coolant, particularly evident at the λ=3d. The distinctive peak performance observed at the centre line in the novel hybrid configuration can be attributed to the disruption of large vortex pairs generated within the console design. This disruption leads to the formation of smaller counter-rotating vortex pairs CRVP and anti-CRVP, resulting in a peak cooling effect at the hole's centerline. Furthermore, subtle adjustments in the positions of the hybrid concept, such as at λ = 2d and λ = 3d for F1, have varying impacts on lateral coolant spreading, with F2 demonstrating enhanced lateral coverage at λ=3d.

3.7 Flow structure

Figures 15 and 16 show the dimensionless temperature contours and streamlines in the Y-Z plane at (x/d = 6) for blowing ratios of B = 0.87 and B = 0.37. Figure 16a. The attached coolant is located between $-1.25<(z/d)<1.25$, exhibiting a stronger presence than at a low blowing ratio of B=0.37, as depicted in Fig. 15a, the stronger CRVP can be observed on the centre-lines of consoles, promoting the mixture between mainstream and secondary flow, resulting in deterioration of film cooling performance, with a small anti-CVRP vortex on the sides, which lifts off away from the end wall. In the context of a novel combined cylinder hole, a significant phenomenon occurs in the disruption of large kidney vortex pairs initially generated within the console, as shown in Figs. 15a and 16a. Large kidney vortex pairs within the console initially exhibit a coherent and sizable rotational motion. However, when this system encounters the influence of the novel combined cylinder hole, especially at larger hole exit areas, the integrity of these large vortex pairs is perturbed. This impact results in the fragmentation of the once-large kidney vortex pairs into two smaller counter-rotating vortices, identified as CRVP. Simultaneously, two anti-CRVP (counter-rotating anti-vortex pair), as shown in Fig. 16b and c structures, are formed due to this disruptive process. This makes the two vortices apart, and the coolant spreads widely. This is particularly evident at high-velocity ratios; conversely, at low-blowing ratios, the momentum of the coolant flow from secondary holes may struggle to penetrate the mainstream flow effectively. This limitation is

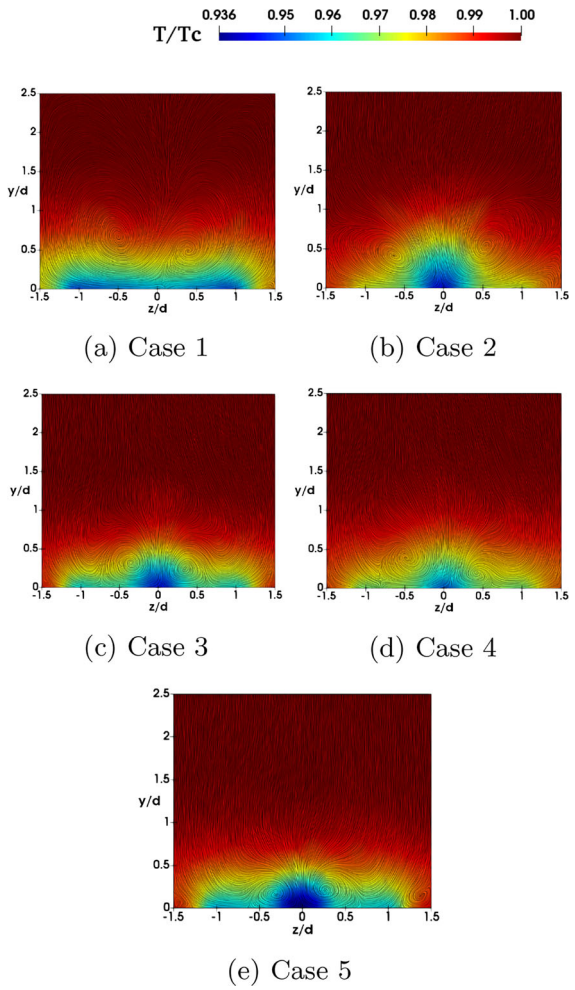

Fig. 15 Dimensionless temperature distributions and streamlines of various configurations in the section of x/d=6 at B=0.37

depicted in Fig. 15b and c, where the branch jet demonstrates inadequate coolant coverage.

The vortices generated by the small secondary holes play a crucial role in enhancing the mixing of coolant with the mainstream flow, as depicted in Fig. 16d and e. Small secondary holes may exhibit distinct interactions with the central hole jet compared to larger secondary holes, influencing the mixing and momentum transfer dynamics. These vortices facilitate improved entrainment and dispersion of the coolant, resulting in a more uniform distribution along the surface, particularly at high blowing ratios. The stronger anti-CRVP generated from the F1, on both sides of the F1, anti-CRVP is seen with reduced intensity compared with the console. The rotation direction of anti—CRVP is contrary to that of CRVP.

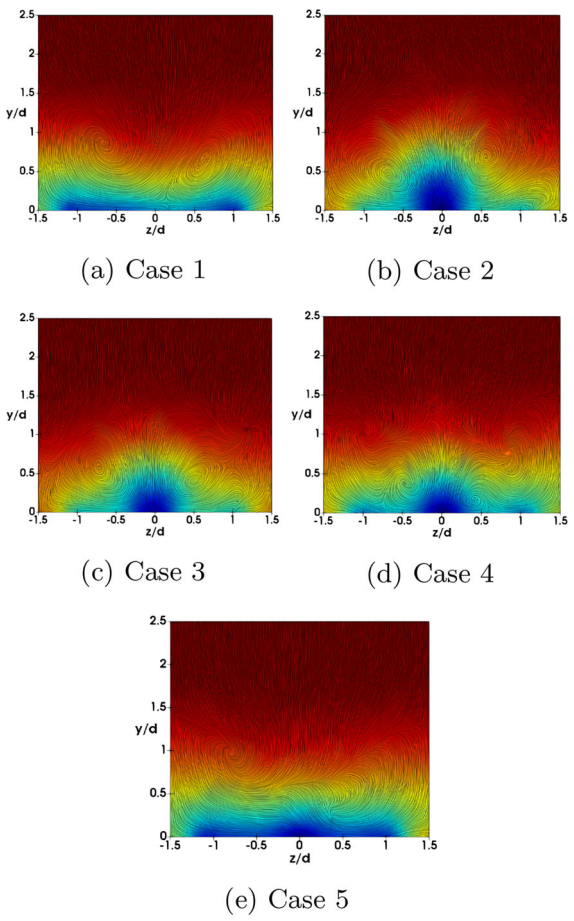

Fig. 16 Dimensionless temperature distributions and streamlines of various configurations in the section of x/d=6 at B=0.87

Moreover, the scale of anti-CRVP is more significant than that of CRVP, especially at λ = 3d, as shown in Fig. 16c. The hybrid film cooling design configuration allows for better coverage of the cooling air over the surface. While this improves overall cooling effectiveness, it also leads to a more distributed flow, reducing the intensity of the counter-rotating vortices.

4 Conclusion

In the present paper, a novel approach to film-cooling hole design has been suggested, and its effectiveness has been evaluated compared to the currently utilized console. They are presenting an original film-cooling innovation called converging slot-hole injection compounds with holes (CCH), which enhances film-cooling efficiency by incorporating additional

branching jets. Additionally, this paper details the impact of auxiliary hole in hybrid cooling approach by examining two positions $\lambda = 2$ and $\lambda = 3$. The results indicate that film cooling effectiveness performs significantly better with novel hybrid film cooling concept CCH. The study's general finding is that the film cooling efficiency increases monotonously with an increasing blowing ratio over a flat surface for all the cases examined. This means that as the blowing ratio of the coolant mass flow rate to the mainstream gas flow rate increases, the film cooling effectiveness improves consistently. Additionally, the area of the exit hole significantly impacts the film cooling effectiveness. F1-CHH with different position holes has been shown to provide the most excellent coverage for film cooling, especially in the downstream region, followed by F2-CCH. The position of the F1-CCH in case 2,3 contributes to expanding the secondary air in the central area, which enhances film cooling coverage. Significantly, the positioning of auxiliary holes profoundly impacts the CRVP structure. It diminishes the lift-off effect of vortices and directs them away from the centre-line plane, facilitating the span-wise spread of coolant flow. Consequently, this configuration effectively curtails the entertainment of mainstream air. The hybrid film cooling approach provides valuable insights into enhancing film cooling technology for gas turbines. While the research identifies limitations related to using flat plate geometry while simplifying the analysis, limits the applicability of the results to actual turbine blade configurations and specific orientation of secondary holes, it also underscores the need to address structural integrity, manufacturability, and optimization challenges in the hybrid scheme design. Despite these limitations, the study's innovative hybrid film cooling approach demonstrates superior effectiveness compared to traditional configurations, positioning it as a significant advancement in gas turbine airfoil performance, especially at high blowing ratios. This research provides practical implications for improving turbine performance and blade protection and sets the stage for future advancements in optimizing film cooling techniques for turbine blade cooling applications. Moreover, all the results presented in this research were obtained using the open-source CFD tool OpenFOAM. Overall, the study's detailed analysis, unique approach, and promising outcomes make it a noteworthy contribution to film cooling with substantial potential for further research and application in gas turbine systems.

References

1. Han JC, Dutta S, Ekkad S (2012) Gas turbine heat transfer and cooling technology. CRC Press, Boca Raton, pp 1–844. https://doi.org/10.1201/b13616
2. Bogard DG, Thole KA (2006) Gas turbine film cooling. J Propul Power 22(2):249–270. https://doi.org/10.2514/1.18034
3. Haven BA, Kurosaka M (1997) Kidney and anti-kidney vortices in crossflow jets. J Fluid Mech 352:27–64. https://doi.org/10.1017/S0022112097007271
4. Tyagi M, Acharya S (2003) Large eddy simulation of film cooling flow from an inclined cylindrical jet. J Turbomach 125(4):734–742. https://doi.org/10.1115/1.1625397
5. Jindal P, Agarwal S, Sharma RP, Roy AK (2018) Enhancement of film cooling effectiveness using rectangular winglet pair. J Therm Sci Eng Appl 10(4):041014. https://doi.org/10.1115/1.4039700
6. Jiang Y, Capone L, Ireland P, Romero E (2018) A detailed study of the interaction between two rows of cooling holes. J Turbomach 140(4):041008. https://doi.org/10.1115/1.4038833
7. Jindal P, Roy A, Sharma R (2016) Effect of hole shapes, orientation and hole arrangements on film cooling effectiveness. Int J Aeronaut Space Sci 17:341–351. https://doi.org/10.5139/IJASS.2016.17.3.341
8. Liu R, Li H, You R, Tao Z, Huang Y (2023) Numerical decoupling of the effect of internal cooling and external film cooling on overall cooling effectiveness. Appl Therm Eng 222:119905. https://doi.org/10.1016/j.applthermaleng.2022.119905
9. Jindal P, Agarwal S, Sharma RP, Roy AK (2017) Numerical investigation of film cooling enhancement using staggered row mixed hole arrangements. J Therm Sci Eng Appl 9(2):021007. https://doi.org/10.1115/1.4035448
10. Abdala AMM, Elwekeel FNM, Qun Z (2012) Comparison of three different two-equation turbulence models in predicting narrow trench film cooling effectiveness. In: Proceedings of the 1st international conference on mechanical engineering and material science (MEMS 2012), pp 713–716. https://doi.org/10.2991/mems.2012.187
11. Acosta WA, Thurman DR, Poinsatte P (2020) Preliminary computational analysis of film cooling on a flat plate at different blowing ratios. Technical Report ARL-TR-8908, U.S. Army Research Laboratory (February)
12. Sargison JE, Guo SM, Oldfield MLG, Lock GD, Rawlinson AJ (2002) A converging slot-hole film-cooling geometry-part 1: low-speed flat-plate heat transfer and loss. J Turbomach 124(3):453–460. https://doi.org/10.1115/1.1459735
13. Doormaal JPV, Raithby GD (1984) Upstream to elliptic problems involving fluid flow. Comput Fluids 2(2):191–220. https://doi.org/10.1080/01495728408961817

14. Menter FR (1994) Two-equation eddy-viscosity turbulence models for engineering applications. AIAA J 32(8):1598–1605. https://doi.org/10.2514/3.12149
15. Wilcox DC (1988) Reassessment of the scale-determining equation for advanced turbulence models. AIAA J 26(11):1299–1310. https://doi.org/10.2514/3.10041
16. Bardina J, Huang P, Coakley T, Bardina J, Huang P, Coakley T, Turbulence modeling validation. https://doi.org/10.2514/6.1997-2121
17. El Ayoubi C (2014) Three-dimensional aero-thermal optimization of film cooling in a high pressure turbine. PhD thesis, Concordia University (May). Unpublished. https://spectrum.library.concordia.ca/id/eprint/978687/